PAPER

Check for updates

The properties and catalytic performance of PtSn/Mg(*x*-Ga)AlO catalysts for ethane dehydrogenation†

Shuqi Fang,[a] Keting Zhang,[a] Chenguang Wang,*[b] Longlong Ma,[b] Qi Zhang,[b] Qiying Liu,[b] Lungang Chen,[b] Lingpeng Chen,[bc] Qiao Zhang[b] and Zhipeng Tian[bc]

Mg(Ga)AlO hydrotalcite materials with different Ga contents are synthesized *via* the coprecipitation method and then used as supports for PtSn/Mg(*x*-Ga)AlO catalysts, in which Pt and Sn nanoparticles are deposited *via* the anion exchange method. The results indicate that a suitable content of Ga evidently enhances the performances and stability of ethane dehydrogenation for the PtSn/Mg(*x*-Ga)AlO catalysts. The S_{BET} of the catalyst increases with the addition of Ga (2–4.5 wt%). The total acidity and strong acid sites decrease significantly when a small quantity of Ga is added. It is favorable for the catalysts to possess a smaller size and better distribution of Pt particles. Moreover, a suitable content of Ga enhances the interaction between Sn and the support and inhibits the reduction of oxidized Sn species, which is helpful to enhance the interaction between the Pt and Sn atoms. The PtSn/Mg(2-Ga)AlO catalyst exhibits the best performance of all the catalysts during the ethane dehydrogenation reaction, with an average ethane conversion of 25.4% for a period of 2 h. No evident activity decrease is observed after 4 cycles of 2 h testing.

1. Introduction

Recently, the demand for light olefins has gradually increased due to their wide use as building blocks in the chemical industry. Steam cracking and fluid catalytic cracking of crude-oil-derived naphtha and other oil byproducts are the traditional methods to obtain light olefins.[1–4] Compared with the traditional methods, the catalytic dehydrogenation of light alkanes exhibits numerous advantages and is more economic and environmentally friendly.[5] However, catalytic dehydrogenation is an endothermic process, and in order to obtain a high yield of olefin, the reaction must be carried out at a relatively high temperature, resulting in the sintering of Pt particles and undesirable side reactions, which are the main reasons for the deactivation of the catalyst.[6,7] Therefore, the development of catalysts with high activity, stability and selectivity is very important.

The performance of catalysts is greatly impacted by their support.[8,9] Al_2O_3 is suggested as a potential support because of

its unique physical properties, such as large surface area and tunable pore size over a wide range. However, since alumina is a type of acidic oxide, deactivation and low selectivity are unavoidable due to its intrinsic strong acid sites. A great amount of research has shown that non-acidic supports, including K–L zeolite, spinels, alkali doped alumina, and calcined hydrotalcite, can greatly enhance the desorption of alkenes and minimize coke formation.[10–12] Among them, calcined hydrotalcite or hydrotalcite-like compounds are seen as ideal supports because they have moderately basic character, high thermal stability and high metal dispersion.[13,14] MgAlO hydrotalcite is a type of layered double hydroxide (LDH), where in the hydrotalcite structure, some Mg^{2+} ions are replaced by Al^{3+} ions, forming positively charged layers. The positive charge is balanced by interlayer anions such as CO_3^{2-}, which are situated between the brucite-like layers. Some divalent and trivalent metal cations can form the same structure as that of hydrotalcite, and is called a hydrotalcite-like compound.[15] It is generally accepted that the ordered crystal structure of LDHs is formed by the supramolecular interactions between the host metal layers and the guest interlayer anions, and this determines the exchangeability of the interlayer anions.[16,17] LDHs with different interlayer inorganic or organic anions can be obtained *via* the ion exchange method, which is useful for the precise synthesis of catalysts.[18]

Platinum is known as the most effective metal for the dehydrogenation of light alkanes.[19] However, without modifiers monometallic Pt supported catalysts exhibit low olefin

[a]*School of Chemical Engineering and Energy, Zhengzhou University, Zhengzhou 450001, P. R. China*

[b]*Key Laboratory of Renewable Energy, Guangzhou Institute of Energy Conversion, Chinese Academy of Sciences, Guangzhou, 510640, P. R. China . E-mail: wangcg@ms.giec.ac.cn; Fax: +86 20 87057789*

[c]*University of Chinese Academy of Sciences, Beijing 100049, P. R. China*

† Electronic supplementary information (ESI) available. See DOI: 10.1039/c7ra00670e

selectivity and deactivate quickly due to the sintering of Pt particles and rapid coke formation.[20,21] To improve the catalyst performance, some bimetallic catalysts were synthesized using doping promoting elements such as Sn, In, Ga, Mn, Zn and Ca.[22,23] Among them, Pt–Sn supported catalysts have been widely researched. The influence of Sn on Pt has been attributed to both geometric and electronic effects.[6] It is well known that the addition of Sn is beneficial for Pt supported catalysts to form smaller Pt particles and a more uniform distribution, reducing the surface Lewis acid sites of the catalysts. Moreover, Sn can also change the interaction between Pt and the support and enhance catalytic stability.[24,25]

Although much attention has been given to Sn as a promoting element, studies have also found that Ga is an effective promoter for propane dehydrogenation.[26,27] Jablonski et al.[28] synthesized a PtGa/Al$_2$O$_3$ catalyst that exhibited higher activity and stability than the Pt/Al$_2$O$_3$ catalyst, and they also found that the catalyst deactivation and carbon deposition were restrained by the addition of Ga. Sun et al.[29,30] synthesized a Pt/Mg(Ga)AlO catalyst using a hydrotalcite material (Mg(Ga)AlO) as the support, and they found that the performance of the catalyst was strongly influenced by the Ga content. Redekop et al.[31] proved that Ga migrates from the surface of the support to the supported Pt nanoparticles to form Pt–Ga alloys, which can make the catalyst more selective and less prone to coking. Homs et al.[32] studied a silica supported PtSn alloy doped with Ga, and observed the electronic modification of the platinum by the Pt–Ga interaction. Wang et al.[33] researched the effect of Ga doping on Pt/CeO$_2$–Al$_2$O$_3$ catalysts for propane dehydrogenation, and they found that Ga improves propylene desorption and greatly suppresses deep dehydrogenation and coke formation. Shao et al.[34] studied the properties and catalytic performance of Ga$_2$O$_3$-based catalysts for the propane dehydrogenation reaction, where the initial propane conversion of the 5Ga$_2$O$_3$/ZSM-5 catalyst reached up to 78.1% at 620 °C and atmospheric pressure.

Since Sn and Ga both have distinct positive effects on the catalyst performance in the dehydrogenation of light alkanes and the synergistic effect between Pt, Sn and Ga is not well studied, herein, a series of hydrotalcite-like materials (Mg(Ga)AlO) is synthesized via the coprecipitation method with different contents of Ga. Pt and Sn nanoparticles are dispersed via the anion exchange method and then applied to the ethane dehydrogenation reaction after reduction. The synthesized catalysts are characterized via several analytical techniques. In addition, the influence of Ga loading on the catalytic performance of the PtSn/Mg(x-Ga)AlO catalysts for ethane dehydrogenation reaction is investigated.

2. Experimental

2.1. Preparation of Mg(x-Ga)AlO supports

The hydrotalcite-like support was synthesized via the coprecipitation method.[35] Briefly, an appropriate amount (Mg^{2+}/Al^{3+} = 2; the loading of Ga was 0, 0.75, 2, 3 and 4.5 wt%) of Mg(NO)$_2$·6H$_2$O, Al(NO)$_3$·9H$_2$O and Ga(NO)$_3$·9H$_2$O were dissolved in 100 mL deionized water to form a mixed metal nitrate solution. Equal volumes of 1.0 M Na$_2$CO$_3$ and 2.0 M NaOH were mixed to form a mixed base solution. Then, these two solutions were mixed by dropwise addition to a reaction vessel containing 200 mL deionized water that was adjusted to pH 10.0 using the mixed base solution in advance. The reaction pH was maintained at 10.0, and the reaction was stirred heavily for the entire process. The entire procedure was carried out at room temperature. Once all of the mixed metal nitrate solution was consumed, an additional amount of 2.0 M NaOH was added to keep the reaction pH at 10.0 for the rest of the precipitation reaction. The mixture was then aged for 12 h at 100 °C with strong stirring. The resulting suspension was filtered, washed with deionized water to neutrality, and dried overnight in air at 100 °C. The dried material was described as hydrotalcite-like Mg(x-Ga)AlO support, where x represents the mass percentage of Ga in the catalysts.

2.2. Preparation of PtSn/Mg(x-Ga)AlO catalysts

PtSn/Mg(x-Ga)AlO catalysts were prepared via the anion exchange method.[36,37] In this method, appropriate amounts (depending on the Pt/Sn molar ratio and Pt wt%) of K$_2$PtCl$_6$ and Na$_2$SnO$_3$ were dissolved in 50 mL deionized water, and the mixed solution was heated at 70 °C. Next, 1 g dried hydrotalcite Mg(x-Ga)AlO was added to the mixed solution and stirred vigorously for 24 h at 70 °C to allow PtCl$_6^{2-}$ and SnO$_3^{2-}$ to sufficiently exchange with CO$_3^{2-}$. After that, the suspension was filtered, washed and dried overnight in air at 100 °C. Then, the samples were reduced by hydrogen at 600 °C to obtain the PtSn/Mg(x-Ga)AlO catalysts. The contents of Pt and Sn were 0.5 wt% and 0.25 wt%.

2.3. Catalyst characterization

2.3.1. XRD. The crystallographic phases of all the supports and catalysts were confirmed by XRD measurements on an X'Pert Pro MPD diffractometer (PW 3040/60) with Cu Kα radiation (0.15 nm), operating at 40 kV and 100 mA. The scanning mode was set at a step of 0.02° and a step counting time of 10 s in the 2θ range from 5° to 80°. The XRD patterns of known compounds are referenced by their corresponding number in the Powder Diffraction File (PDF) database.

2.3.2. BET. N$_2$ adsorption–desorption at liquid nitrogen temperature was used to measure the textural properties of the PtSn/Mg(x-Ga)(Al)O catalysts on an automatic analyzer (ASAP 2010, Micrometritics, USA). Before adsorption, the samples were degassed for 10 h at 300 °C. The BET (Brunauer–Emmett–Teller) surface areas of the samples were calculated using the BET multi-points method. The porous volumes were calculated using the BJH (Barrett–Joyner–Halenda) method with Halsey equation for multilayer thickness.

2.3.3. NH$_3$-TPD. Temperature programmed desorption of ammonia (NH$_3$-TPD) measurements were implemented to analyze the acidity of the catalysts. About 0.1 g sample was placed in a quartz reactor between two quartz wool plugs. Before NH$_3$ adsorption, the sample was reduced by hydrogen (H$_2$/Ar = 1/19, 30 mL min^{-1}) at 600 °C for 1 h. Then, the sample was saturated with NH$_3$ at 120 °C. Subsequently, a thermal

conductivity detector (TCD) was used to detect the NH_3-TPD profile from 120 to 600 °C at the rate of 5 °C min^{-1}.

2.3.4. XPS. XPS (X-ray photoelectron spectroscopy) measurements were conducted on an ESCALAB 250Xi spectrometer (Thermo Electron Corp. Altrincham, UK) with an Al Kα source (1486.6 eV), and all the binding energies of Sn were revised according to the C 1s peak at 284.8 eV.

2.3.5. SEM. The morphologies of the catalysts were examined *via* field emission scanning electron microscopy (SEM, SU-70) operated at 5.0 kV.

2.3.6. TEM. Transmission electron microscopy (TEM) images of the catalysts were taken with a JEM-20100F microscope operated at 200 kV. The samples after reductive treatment were dispersed and sonicated in ethanol. Then, a small drop of the dispersion was placed on a carbon film coated copper grid, and dried in air before testing. More than one hundred individual metal particles were collected for the determination of average particle size of each sample.

2.4. Direct dehydrogenation of ethane

The ethane direct dehydrogenation reactions of the different catalysts were carried out in a fixed-bed quartz reactor with an inner diameter of 8 mm under atmospheric pressure. The catalyst (100 mg) was placed in the center of reactor and reduced in an atmosphere of 10% H_2/N_2 at 600 °C for 3 h. Then, a feed containing C_2H_6 and N_2 (molar ratio of $C_2H_6/N_2 = 0.25$, WHSV = 12.9 h^{-1}) was used to determine the activity, selectivity and stability of all the PtSn/Mg(x-Ga)AlO catalysts. The ethane dehydrogenation reactions were carried out at 550 °C. The reaction products were analyzed online using a gas chromatography-mass spectrometer (GC-MS, Agilent 7890B). A flame ionization detector (FID) was used to quantify the concentrations of all organic compounds eluting from the capillary column. A thermal conductivity detector (TCD) was used to quantify H_2, CO and N_2. The ethane conversion and ethylene selectivity are defined as follows:

$$C_2H_6 \ \text{conversion} = \frac{C_2H_{6_{in}} - C_2H_{6_{out}}}{C_2H_{6_{in}}} \times 100\% \qquad (1)$$

$$C_2H_4 \ \text{selectivity} = \frac{C_2H_{4_{out}}}{C_2H_{6_{in}} - C_2H_{6_{out}}} \times 100\% \qquad (2)$$

where $C_2H_{6_{in}}$ and $C_2H_{6_{out}}$ are the ethane content in the feed and exit gases, respectively, and $C_2H_{4_{out}}$ is the ethylene content in the exit gas.

3. Results and discussion

3.1. Characterization of the samples

3.1.1. XRD patterns of the samples. Fig. 1a shows the XRD patterns of the different hydrotalcite-like Mg(x-Ga)AlO. Notably, the diffraction peaks of (003), (006), (110) and (113) are detected over the hydrotalcite-like Mg(x-Ga)AlO, which can be ascribed to the characteristic peaks of hydrotalcite materials.[38] All the diffraction peaks are very narrow and sharp, which reflect high crystallinity and good hydrotalcite structure. The basal spacing
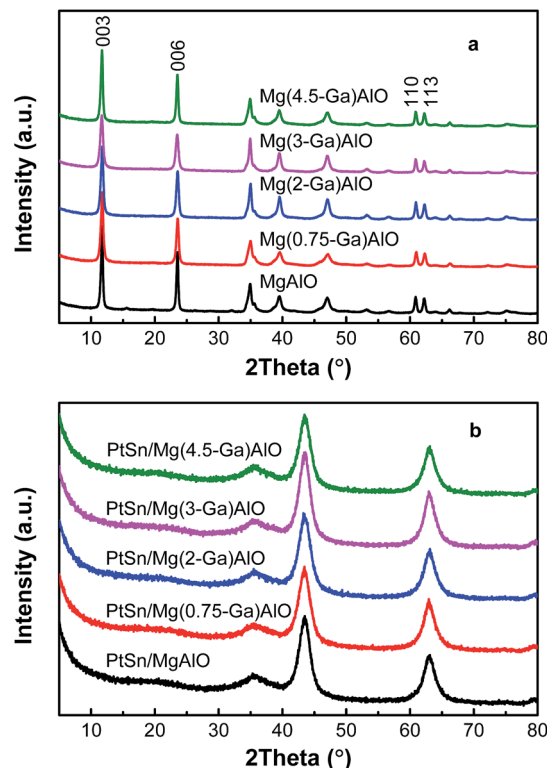

Fig. 1 X-ray diffraction patterns for (a) hydrotalcite-like Mg(x-Ga)AlO and (b) PtSn/Mg(x-Ga)AlO catalysts.

of (003) is about 0.75–0.76 nm, which indicates that CO_3^{2-} is the interlayer anion. There is no difference in the distance of the (110) plane for all the samples which is a reflection of the average charge of the metal cations.

The XRD patterns of the catalysts are illustrated in Fig. 1b. As can be seen, all the characteristic diffraction peaks of the hydrotalcite material disappear and only characteristic diffraction peaks corresponding to MgO are observed. The reason for this is that the structure changes from a two-dimensional layered structure to a three-dimensional structure. The diffraction peaks of Al, Ga, Al_2O_3 or Ga_2O_3 species were not detected for all the catalysts because Al and Ga are highly dispersed in the LDHs during the synthetic process and located in the interstitial sites in the MgO framework after calcination;[39] thus the crystal structure of MgO was not destroyed by the addition of Al and Ga. Moreover, the diffraction peaks of Pt and Sn species are also not detected since their small particle size and/ or low concentration is lower than the XRD detection limitation.[40]

3.1.2. Textural properties of the samples. Low temperature nitrogen adsorption–desorption experiments were carried out to determine the textural properties of the PtSn/Mg(x-Ga)AlO catalysts. As can be seen from Fig. 2, all the catalysts exhibit the same typical type IV adsorption isotherms, which indicate typical mesoporous materials.[41] The textural properties are shown in Table 1. It can be noted that, when the Ga content increases from 0.75% to 2%, there is a great increase in S_{BET} and V_P, which indicates that the structure of the catalysts was
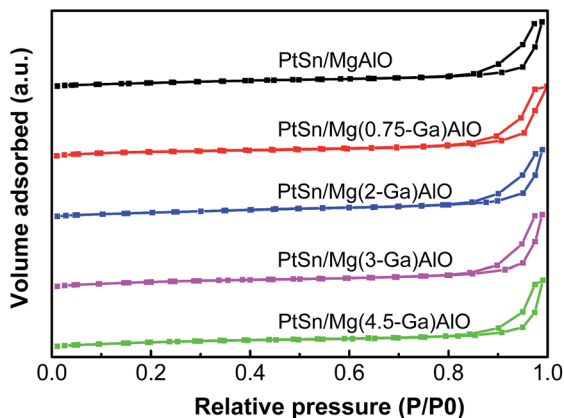
Fig. 2 Low temperature N_2 adsorption–desorption isotherms of the PtSn/Mg(x-Ga)AlO catalysts.

Fig. 3 NH$_3$-TPD profiles of the PtSn/Mg(x-Ga)AlO catalysts: (a) PtSn/MgAlO, (b) PtSn/Mg(0.75-Ga)AlO, (c) PtSn/Mg(2-Ga)AlO, (d) PtSn/Mg(3-Ga)AlO and (e) PtSn/Mg(4.5-Ga)AlO.

Table 1 Compositions and textural properties of the PtSn/Mg(x-Ga)AlO catalysts

Catalyst	Loadings (wt%)		S_{BET} (m^2 g^{-1})	V_p (cm^3 g^{-1})
	Pt	Sn		
PtSn/MgAlO	0.34	0.19	212.7	0.80
PtSn/Mg(0.75-Ga)AlO	0.49	0.21	215.8	0.75
PtSn/Mg(2-Ga)AlO	0.47	0.21	276.4	0.96
PtSn/Mg(3-Ga)AlO	0.49	0.22	273.3	0.94
PtSn/Mg(4.5-Ga)AlO	0.46	0.20	278.2	0.96

changed to some extent, thus making it easier for hydrotalcite to form thin sheet particles, resulting in an increase in S_{BET} and V_p.

3.1.3. Surface acidity analysis. It was reported that the catalyst performance for ethane dehydrogenation is closely related to the number and strength of acid sites on the catalyst surface, particularly strong acid sites which are the main reason for side reactions (cracking, isomerization and polymerization).[23,42] The acidic properties of the catalysts were investigated *via* temperature programmed desorption of NH_3 (NH_3-TPD). The NH_3-TPD curves of the PtSn/Mg(x-Ga)AlO catalysts are illustrated in Fig. 3. The semi-quantitative analysis of the acidity strength distribution was acquired using the Gaussian curve fitting method.[43] The total acidity and acidity strength distribution of the catalysts is listed in Table 2. As can be seen from Fig. 3, all the catalysts exhibit a similar broad desorption shape consisting of three peaks at around 220 °C, 320 °C and 450 °C. According to a previous study, the three fitted peaks are regarded as weak, medium, and strong acid sites, respectively, which should be attributed to the Lewis acidity of the MgO–Al$_2$O$_3$ mixed oxide.[44] From Table 2, it can be noticed that when a small quantity of Ga was added, the total acidity and the fraction of strong acid sites distinctly decreased. The PtSn/Mg(0.75-Ga)AlO catalyst exhibits the lowest total acidity and the PtSn/Mg(2-Ga)AlO catalyst possesses the lowest fraction of strong acid sites. It must be noted that the values increase with an increase in Ga
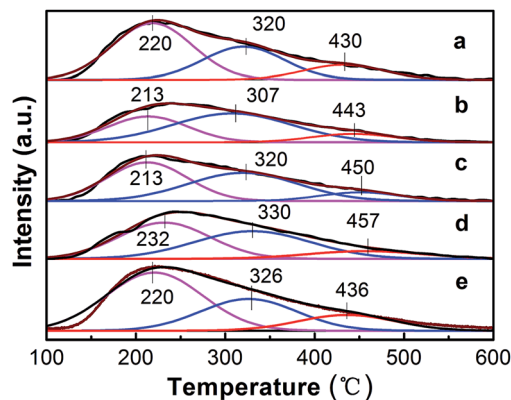
content; therefore the PtSn/Mg(4.5-Ga)AlO catalyst has the highest total acidity and the highest fraction of strong acid sites. This can be explained by the fact that Ga is a type of alkali and can reduce the acidity of the catalysts.[45] In turn, the excess Ga replaces Mg, and this leads to an increase in acidity. These results suggest that the content of Ga can markedly influence the acidity of the catalysts. The PtSn/Mg(2-Ga)AlO catalyst possesses the lowest fraction of strong acid sites and relatively low total acidity.

3.1.4. XPS analysis of the catalysts. The XPS Sn $3d_{5/2}$ spectra of the PtSn/Mg(x-Ga)AlO catalysts are shown in Fig. 4. The deconvolution results of the corresponding spectra are summarized in Table 3. It can be seen that the Sn $3d_{5/2}$ XPS spectra of all the reduced PtSn/Mg(x-Ga)AlO catalysts can be deconvoluted into three peaks at ~485.27 eV, ~486.50 eV and ~487.55 eV, which represent different types of tin species. The peak at ~485.27 eV corresponds to the reduced tin species (Sn^0); whereas the peaks at ~486.50 eV and ~487.55 eV are assigned to the oxidized tin species (Sn^{2+} and Sn^{4+}).[46] From Fig. 4 it can be seen that the binding energy of Sn^0 and Sn^{4+} is evidently skewed by about 0.26 eV and 0.36 eV, respectively, when comparing the PtSn/MgAlO catalyst with the PtSn/Mg(4.5-Ga)AlO catalyst, and the binding energy of Sn^{4+} increases gradually with the increase in Ga loading. From Table 3, it is found that the percentage of Sn^0 for PtSn/MgAlO is 26.8%. When a small amount of Ga was added to the PtSn/Mg(x-Ga)AlO catalyst, the percentage of Sn^0 decreased with the increase in Ga content; the percentage of Sn^0 in the PtSn/Mg(0.75-Ga)AlO and PtSn/Mg(2-Ga)AlO catalysts is about 23.82% and 21.28%, respectively. However, with a further increase in Ga, Sn^0 also increases; the percentage of Sn^0 in the PtSn/Mg(3-Ga)AlO and PtSn/Mg(4.5-Ga)AlO catalysts is about 26.53% and 27.17%, respectively. All these results verify that Ga can electronic modify the tin valency, thus proper amount of Ga can inhibit the reduction and stabilize the oxidation states of tin species, which is beneficial to strengthen the Pt–Sn and Sn–support interactions.[47] The XPS spectra of Ga 2p for the reduced PtSn/Mg(2-Ga)AlO catalyst are shown in Fig. S1,† in which only the peaks for Ga$_2$O$_3$ are observed. Thus, we consider that Ga was not reduced and was still present in the oxidic state.

Table 2 Summary of the NH_3-TPD measurements

Catalyst	Peak temperature (°C)			Peak area fraction (%)			Total area (a.u.)
	Peak I	Peak II	Peak III	Peak I	Peak II	Peak III	
PtSn/MgAlO	220	320	430	55	30	15	785.46
PtSn/Mg(0.75-Ga)AlO	213	307	443	55	34	11	561.11
PtSn/Mg(2-Ga)AlO	213	320	450	45	45	10	650.7
PtSn/Mg(3-Ga)AlO	232	330	457	44	44	12	673.7
PtSn/Mg(4.5-Ga)AlO	220	326	436	55	30	15	1002.5
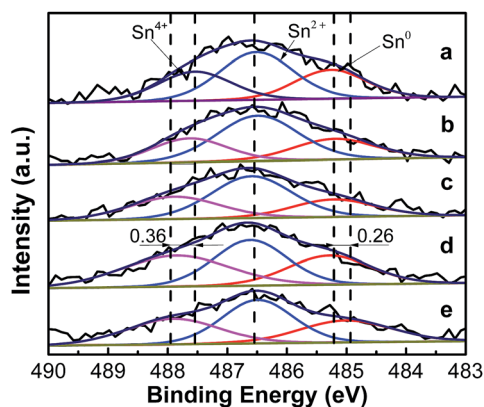
Fig. 4 Sn $3d_{5/2}$ XPS profiles of PtSn/Mg(x-Ga)AlO catalysts: (a) PtSn/MgAlO, (b) PtSn/Mg(0.75-Ga)AlO, (c) PtSn/Mg(2-Ga)AlO, (d) PtSn/Mg(3-Ga)AlO, and (e) PtSn/Mg(4.5-Ga)AlO.
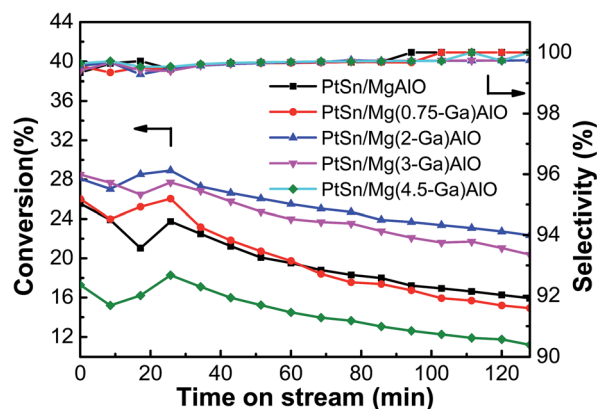
Fig. 5 Effect of the Ga loading of the PtSn/Mg(x-Ga)AlO catalysts on their catalytic performance in ethane dehydrogenation (reaction conditions: T = 550 °C; C_2H_6/N_2 = 0.25; WHSV = 12.9 h^{-1}; and m_{cat} = 100 mg).

3.2. Catalytic performances in ethane dehydrogenation

3.2.1. Effect of Ga content. The ethane conversion and ethylene selectivity over the PtSn/Mg(x-Ga)AlO catalysts are shown in Fig. 5. It was observed that all the catalysts initially exhibited a gradually stable process. The ethane conversion peaked at about 0.5 h and then began to descend slowly. The average ethane conversion of the PtSn/MgAlO catalyst was 19.7%, and with an increase in Ga loading, the conversion of ethane increased markedly. The average ethane conversion increased to 25.4% for the PtSn/Mg(2-Ga)AlO catalyst, which is an improvement of about 28.9% compared with the PtSn/MgAlO catalyst. However the ethane conversion decreased evidently as the Ga loading further increased to above 3 wt%. The average ethane conversion decreased to 14.4% for the PtSn/Mg(4.5-Ga)AlO catalyst, which is lower than that of the PtSn/

MgAlO catalyst, indicating that an excess content of Ga in the PtSn/Mg(x-Ga)AlO catalysts is disadvantageous for ethane conversion, which is consistent with the structure and surface properties in the previous sections. All the catalysts exhibited relatively high selectivity (>99%) during the entire dehydrogenation process, which verifies that the addition of Ga has no evident influence on the catalyst selectivity.

The results indicate that the presence of Ga has an evident impact on the ethane dehydrogenation performances of the PtSn/Mg(x-Ga)AlO catalysts. This can be explained as follows: first, according to the low temperature nitrogen adsorption–desorption experimental results in Table 2, we know that the addition of Ga can change the structure of the catalysts to some extent, leading to an increase in the S_{BET} value of the PtSn/Mg(x-

Table 3 Summary of the XPS results of the PtSn/Mg(x-Ga)AlO catalysts

	BE[a] (eV)				
	PtSn/MgAlO	PtSn/Mg(0.75-Ga)AlO	PtSn/Mg(2-Ga)AlO	PtSn/Mg(3-Ga)AlO	PtSn/Mg(4.5-Ga)AlO
Sn^0	485.27 (26.8%)	485.20 (23.82%)	485.22 (21.28%)	485.29 (26.53%)	485.01 (27.17%)
Sn^{2+}	486.51 (45.45%)	486.49 (51.44%)	486.59 (49.34%)	486.61 (36.73%)	486.49 (41.25%)
Sn^{4+}	487.55 (27.74%)	487.63 (24.74%)	487.88 (29.37%)	487.86 (36.74%)	487.91 (31.59%)

[a] BE: binding energy.

Ga)AlO catalysts, resulting in a better distribution of Pt particles, more Pt active reaction sites and better performances of ethane dehydrogenation.[48]

According to the NH_3-TPD results, Ga can reduce the acidity of the catalysts, particularly the strong acid sites which is the main reason for side reactions. Therefore, it can effectively suppress the undesired side reactions for ethane dehydrogenation and improve the ethane conversion and ethylene selectivity. According to previous research, the PtSn/Mg(x-Ga)Al catalyst is bifunctional, and its two active centers (the metal particle and the acid site) work collaboratively. An optimum ratio exists between the number of metal active sites and the number of acid sites.[49] The ratio between the support acid sites and the number of metal sites of the PtSn/Mg(x-Ga)Al catalyst may change by the addition of Ga so that a better catalytic performance can be obtained. Perhaps the PtSn/Mg(2-Ga)Al catalyst possesses an optimum ratio between the two types of sites.

According to previous research, the state of Sn has a significant influence on the performance of the catalytic properties of Pt. Metallic Sn has an evident inhibiting effect on the catalyst performance. However, when it exists in the oxidized state, it acts as a promoter.[47] The XPS results indicate that the PtSn/Mg(2-Ga)Al catalyst has the lowest percent of tin metal and the highest percent of oxidation states of Sn species.

The micrographs of the hydrotalcite-like crystals obtained by SEM analysis are shown in Fig. 6, where great differences can be observed between MgAlO and Mg(2-Ga)AlO. It can be seen that the former exhibits mainly small tabular particles with a flake-like structure mixed in it, whereas the latter is formed mainly by a flake-like structure with a thickness of 10 nm; thus the addition of Ga causes hydrotalcite to form a more regular layer structure. The SEM image of the reduced PtSn/Mg(2-Ga)AlO catalyst is shown in Fig. S2,† in which some hydrotalcite layers are still observed. Therefore, it can be concluded that the structure of the catalysts was changed by the addition of Ga, which is in accordance with the BET results.

The morphology and metal particle size of PtSn/Mg(x-Ga)AlO were characterized by TEM in Fig. 7. It can be seen that the PtSn/
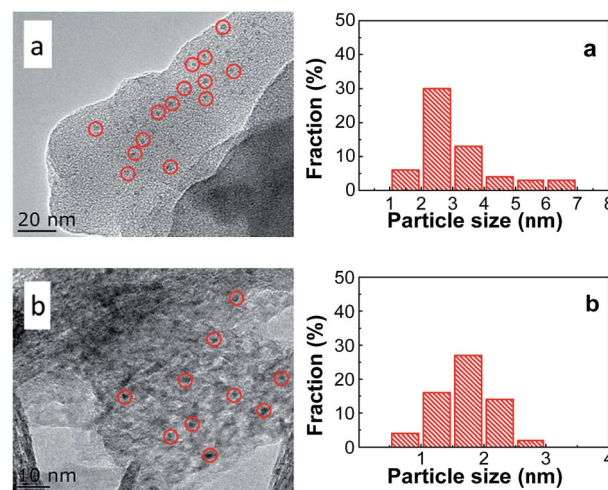

Fig. 7 TEM images and the corresponding particle size distributions of (a) PtSn/MgAlO and (b) PtSn/MgGa$_2$AlO.

Mg(2-Ga)AlO catalyst has a smaller average metal particle size (1.69 nm) than the 0.5PtSn/MgAlO catalyst (3.12 nm), and it exhibits a better distribution of Pt particles, which indicates that the addition of a certain amount of Ga is beneficial for the formation of small Pt particles and their uniform distribution. This can be explained as follows: on one hand, the presence of Ga has a dilution effect on platinum, which is conducive to decrease the size of the Pt particles.[10] On the other hand, the addition of Ga can promote hydrotalcite to form more regular thin sheet particles, and thus a more thorough iron exchange can occur, which is beneficial for the uniform distribution of the Pt component on the support. According to previous research, smaller Pt particles and their better distribution can supply more Pt active reaction sites and inhibit the hydrogen and carbon deposition reaction at the same time. This is because hydrogen and carbon deposition are structure sensitive reactions that require big Pt particles.

3.2.2. Effect of temperature. The effect of reaction temperature on the performance of the PtSn/Mg(2-Ga)AlO catalyst in ethane dehydrogenation was investigated, and the results are shown in Fig. 8. All the catalysts exhibit relatively high selectivity (>99%) during the entire dehydrogenation process. The initial ethane conversions are 18.1%, 28.1% and 32.8% at the reaction temperatures of 500, 550 and 600 °C, which decrease to 15.6%, 22.3% and 13.2% after 128 min reaction, respectively. The highest initial ethane conversion was obtained at the reaction temperature of 600 °C. However, the activity and stability declined very quickly because thermal cracking was enhanced at high temperature, which led to carbon deposition on the catalyst surface. When the reaction is performed at a lower temperature, such as 500 °C, the catalyst exhibits the best stability and the ethane conversion only decreases by 13.8%; however, the average ethane conversion is too low. An average conversion of 25.4% was acquired at 550 °C, which is certainly higher than that at 500 and 600 °C. To balance the conversion and stability of ethane
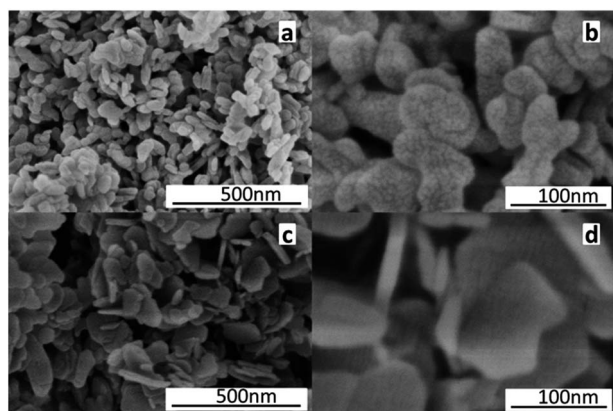

Fig. 6 SEM images of the hydrotalcite-like support: (a and b) MgAlO, and (c and d) Mg(2-Ga)AlO.
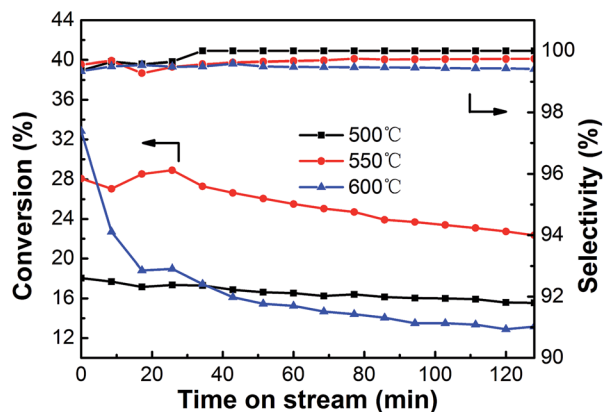
Fig. 8 The effect of temperature on the catalytic performance of PtSn/Mg(2-Ga)AlO catalyst (reaction conditions: $C_2H_6/N_2 = 0.25$; WHSV = 12.9 h^{-1}; m_{cat} = 100 mg).

Fig. 10 Stability tests of the PtSn/Mg(2-Ga)AlO and PtSn/MgAlO catalysts in ethane dehydrogenation (reaction conditions: T = 550 °C; $C_2H_6/N_2 = 0.25$; WHSV = 12.9 h^{-1}; and m_{cat} = 100 mg).
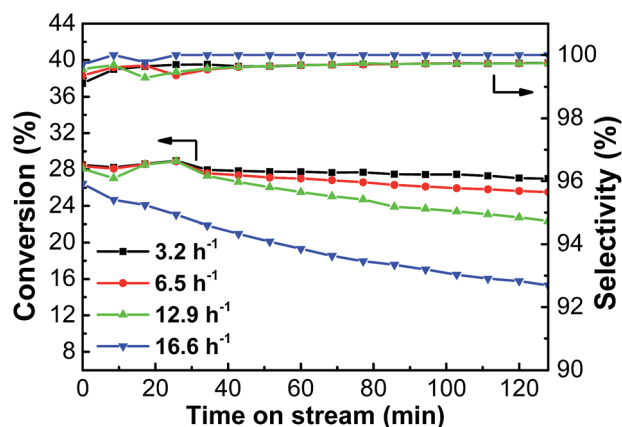

Fig. 9 The effect of WHSV on the catalytic performance of PtSn/Mg(2-Ga)AlO catalyst (reaction conditions: T = 550 °C; $C_2H_6/N_2 = 0.25$; m_{cat} = 100 mg).

Fig. 11 The catalytic performances of PtSn/Mg(2-Ga)AlO catalysts within 4 reaction-regeneration cycles (reaction conditions: T = 550 °C; $C_2H_6/N_2 = 0.25$; WHSV = 12.9 h^{-1}; m_{cat} = 100 mg).

dehydrogenation, the reaction temperature of 550 °C is the desired selection.

3.2.3. Effect of WHSV. Fig. 9 shows the conversion and selectivity of the PtSn/Mg(2-Ga)AlO catalyst for ethane the dehydrogenation reaction with different WHSV. As can be seen, the highest average ethane conversion of 27.1% was obtained at 3.2 h^{-1}. The average ethane conversion decreased with an increase in GHSV; nevertheless, the decrease was very small. However, when the GHSV increased to 16.6 h^{-1}, the ethane conversion decreased evidently due to the fact that the contact time between ethane and the catalyst was shortened, and the reaction did not proceed adequately.

3.2.4. Stability test. Stability tests for the PtSn/Mg(2-Ga)AlO and 0.5PtSn/MgAlO catalysts were carried out, and the ethane conversion and ethylene selectivity for ethane dehydrogenation are shown in Fig. 10. The ethane conversion of the PtSn/Mg(2-Ga)AlO and PtSn/MgAlO catalysts decreased to 31.3% and 66.8% after 14 h reaction, and their final catalytic activities were 19.3% and 8.2%, respectively. The catalyst stability was greatly enhanced by the addition of Ga because Ga can reduce the
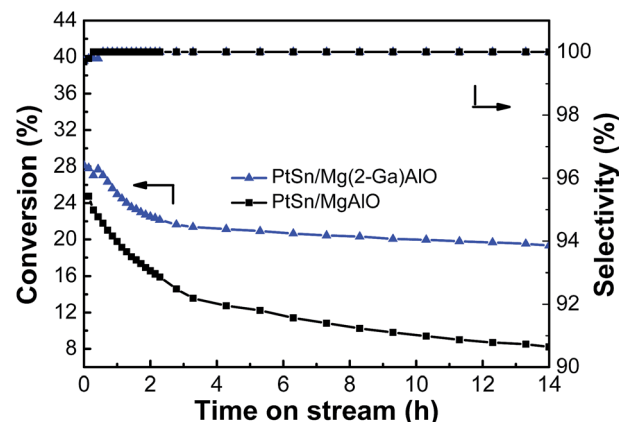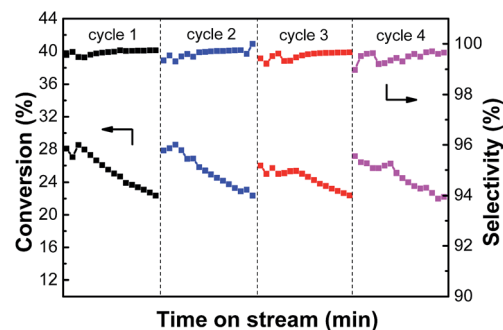
deactivation and the coke accumulation.[30] The selectivity of both catalysts was above 99% during the entire reaction process.

3.2.5. The reaction-regeneration of PtSn/Mg(2-Ga)AlO catalyst. A reaction–regeneration test for the PtSn/Mg(2-Ga)AlO catalyst was carried out to investigate the effects of reduction–reaction–oxidation cycles on catalyst activity during ethane dehydrogenation. It can be seen from Fig. 11 that in each cycle, the catalyst has a stable stage and then the ethane conversion gradually decreases. During the 4 cycles, the average ethane conversions are 25.4%, 25.4%, 24.4 and 24.6%. No significant activity decrease was observed after 4 cycles, and the ethylene selectivity varied a little at about 99% in each cycle period. Thus, we propose that the main reason for the loss in catalyst activity was not the sintering of the metal particles but carbon deposition on the catalyst surface. The coke can be fully removed by oxidation and the catalyst activity can be restored by subsequent reduction.

4. Conclusions

Hydrotalcite Mg(x-Ga)AlO materials were synthesized *via* the coprecipitation method with a constant pH, and PtSn/Mg(x-Ga)

AlO catalysts were prepared *via* the anion exchange method. The XRD, BET and SEM measurements show that the structure of the catalysts changed to some extent on the addition of Ga, but the crystal structure was not destroyed. The NH_3-TPD results suggest that a moderate amount of Ga can markedly neutralize the acid sites of the catalysts and effectively suppress the undesired side reactions for ethane dehydrogenation. The TEM measurements show that the addition of Ga in the catalyst is beneficial for the formation of small Pt particles and their uniform distribution. The average particle size of the PtSn/Mg(2-Ga)AlO catalyst is 1.69 nm. The XPS results verify that the suitable Ga content can strengthen the Sn–support and Pt–Sn interactions, which can enhance the properties of the catalysts. The PtSn/Mg(2-Ga)AlO catalyst exhibits the best ethane dehydrogenation performance. The ethane conversion of the PtSn/Mg(2-Ga)AlO catalyst varies from 25.6% to 17.0% in a 14 h ethane dehydrogenation reaction. The catalyst performance has no evident decline after 4 reaction–regeneration cycles with selectivity above 99% for each cycle.

Acknowledgements

Notes and references

1 N. A. Pakhomov, V. N. Kashkin, E. I. Nemykina, V. V. Molchanov, V. I. Nadtochiy and A. S. Noskov, *Chem. Eng. J.*, 2009, **154**, 185–188.

2 F. Cavani, N. Ballarini and A. Cericola, *Catal. Today*, 2007, **127**, 113–131.

3 R. S. Vincent, R. P. Lindstedt, N. A. Malik, I. A. B. Reid and B. E. Messenger, *J. Catal.*, 2008, **260**, 37–64.

4 J. J. Sattler, J. Ruiz-Martinez, E. Santillan-Jimenez and B. M. Weckhuysen, *Chem. Rev.*, 2014, **114**, 10613.

5 L. Shi, G. M. Deng, W. C. Li, S. Miao, Q. N. Wang, W. P. Zhang and A. H. Lu, *Angew. Chem.*, 2015, **54**, 13994–13998.

6 K. Kumbilieva, N. A. Gaidai, N. V. Nekrasov, L. Petrov and A. L. Lapidus, *Chem. Eng. J.*, 2006, **120**, 25–32.

7 B. K. Vu, M. B. Song, I. Y. Ahn, Y.-W. Suh, D. J. Suh, W.-I. Kim, H.-L. Koh, Y. G. Choi and E. W. Shin, *Appl. Catal., A*, 2011, **400**, 25–33.

8 J. Silvestre-Albero, J. C. Serrano-Ruiz, A. Sepúlveda-Escribano and F. Rodríguez-Reinoso, *Appl. Catal., A*, 2008, **351**, 16–23.

9 Y. Zhang, Y. Zhou, J. Shi, S. Zhou, X. Sheng, Z. Zhang and S. Xiang, *J. Mol. Catal. A: Chem.*, 2014, **381**, 138–147.

10 S. A. Bocanegra, A. A. Castro, O. A. Scelza and S. R. de Miguel, *Appl. Catal., A*, 2007, **333**, 49–56.

11 M. P. Lobera, C. Téllez, J. Herguido and M. Menéndez, *Appl. Catal., A*, 2008, **349**, 156–164.

12 A. Virnovskaia, S. Morandi, E. Rytter, A. Giovanna Ghiotti and U. Olsbye, *J. Phys. Chem. C*, 2007, **111**, 14732–14742.

13 J. I. D. Cosimo, V. K. DíEz, M. Xu, E. Iglesia and C. R. ApesteguíA, *J. Catal.*, 1998, **178**, 499–510.

14 J. H. Kwak, J. Hu, D. Mei, C.-W. Yi, D. H. Kim, C. H. F. Peden, L. F. Allard and J. Szanyi, *Science*, 2009, **325**, 1670–1673.

15 R. L. Frost, S. J. Palmer and L.-M. Grand, *J. Raman Spectrosc.*, 2010, **41**, 1797–1802.

16 J. T. Kloprogge, D. Wharton, L. Hickey and R. L. Frost, *Am. Mineral.*, 2002, **87**, 623–629.

17 S. Miyata, *Clays Clay Miner.*, 1983, **31**, 305–311.

18 J. H. Lee, S. W. Rhee and D. Y. Jung, *Chem. Mater.*, 2004, **16**, 3774–3779.

19 B. Y. Jibril, A. Atta, K. Melghit, Z. El-Hadi and H. Ala'a, *Chem. Eng. J.*, 2012, **193**, 391–395.

20 Y. Zhang, Y. Zhou, J. Shi, X. Sheng, Y. Duan, S. Zhou and Z. Zhang, *Fuel Process. Technol.*, 2012, **96**, 220–227.

21 P. Sun, G. Siddiqi, W. C. Vining, M. Chi and A. T. Bell, *J. Catal.*, 2011, **282**, 165–174.

22 J. Wu, Z. Peng and A. T. Bell, *J. Catal.*, 2014, **311**, 161–168.

23 C. Yu, H. Xu, Q. Ge and W. Li, *J. Mol. Catal. A: Chem.*, 2007, **266**, 80–87.

24 V. Galvita, G. Siddiqi, P. Sun and A. T. Bell, *J. Catal.*, 2010, **271**, 209–219.

25 K. Xia, W.-Z. Lang, P.-P. Li, L.-L. Long, X. Yan and Y.-J. Guo, *Chem. Eng. J.*, 2016, **284**, 1068–1079.

26 K. Searles, G. Siddiqi, O. V. Safonova and C. Copéret, *Chem. Sci.*, 2017, **8**, 2661–2666.

27 R. Koirala, R. Buechel, F. Krumeich, S. E. Pratsinis and A. Baiker, *ACS Catal.*, 2015, **5**, 690–702.

28 E. Jablonski, A. Castro, O. Scelza and S. De Miguel, *Appl. Catal., A*, 1999, **183**, 189–198.

29 P. Sun, G. Siddiqi, M. Chi and A. T. Bell, *J. Catal.*, 2010, **274**, 192–199.

30 G. Siddiqi, P. Sun, V. Galvita and A. T. Bell, *J. Catal.*, 2010, **274**, 200–206.

31 E. A. Redekop, V. V. Galvita, H. Poelman, V. Bliznuk, C. Detavernier and G. B. Marin, *ACS Catal.*, 2014, **4**, 1812–1824.

32 N. S. Homs, J. Llorca, M. Riera, J. Jolis, J.-L. G. Fierro, J. Sales and P. R. R. de la Piscina, *J. Mol. Catal. A: Chem.*, 2003, **200**, 251–259.

33 T. Wang, F. Jiang, G. Liu, L. Zeng, Z. J. Zhao and J. Gong, *AIChE J.*, 2016, **62**, 4365–4376.

34 C. T. Shao, W. Z. Lang, X. Yan and Y. J. Guo, *Rsc Adv.*, 2017, **7**, 4710–4723.

35 S. K. Yun and T. J. Pinnavaia, *Chem. Mater.*, 1995, **7**, 348–354.

36 O. Altuntasoglu, U. Unal, S. Ida, M. Goto and Y. Matsumoto, *J. Solid State Chem.*, 2008, **181**, 3257–3263.

37 L. P. Chen, Z. P. Tian, W. Lv, Z. Si, Q. Y. Liu, M. Y. Ding, L. G. Chen, L. L. Ma, Q. Zhang, T. J. Wang and C. G. Wang, *J. Fuel Chem. Technol.*, 2016, **44**, 597–606.

38 Y. Lin, J. Wang, D. G. Evans and D. Li, *J. Phys. Chem. Solids*, 2006, **67**, 998–1001.

39 J. A. van Bokhoven, J. Roelofs, K. P. de Jong and D. C. Koningsberger, *Chem.–Eur. J.*, 2001, **7**, 1258–1265.

40 Y. W. Zhang, Y. M. Zhou, X. L. Sheng, L. H. Wan, Y. J. Li, Y. M. Xiao, B. Yu and Z. Zeng, *Fuel Process. Technol.*, 2012, **104**, 23–30.

41 B. Xu, J. Long, H. Tian, Y. Zhu and X. Sun, *Catal. Today*, 2009, **147**, S46–S50.

42 X. Liu, W.-Z. Lang, L.-L. Long, C.-L. Hu, L.-F. Chu and Y.-J. Guo, *Chem. Eng. J.*, 2014, **247**, 183–192.

43 C. Yu, Q. Ge, H. Xu and W. Li, *Appl. Catal., A*, 2006, **315**, 58–67.

44 R. J. Balasamy, B. B. Tope, A. Khurshid, A. A. S. Al-Ali, L. A. Atanda, K. Sagata, M. Asamoto, H. Yahiro, K. Nomura, T. Sano, K. Takehira and S. S. Al-Khattaf, *Appl. Catal., A*, 2011, **398**, 113–122.

45 F. B. Passos, D. A. Aranda and M. Schmal, *J. Catal.*, 1998, **178**, 478–488.

46 A. D. Ballarini, C. G. Ricci, S. R. de Miguel and O. A. Scelza, *Catal. Today*, 2008, **133**, 28–34.

47 J. Shi, Y. Zhou, Y. Zhang, S. Zhou, Z. Zhang, J. Kong and M. Guo, *J. Mater. Sci.*, 2014, **49**, 5772–5781.

48 K. Xia, W.-Z. Lang, P.-P. Li, X. Yan and Y.-J. Guo, *Rsc. Adv.*, 2015, **5**, 64689–64695.

49 M. Larsson, M. Hulten, E. A. Blekkan and B. Andersson, *J. Catal.*, 1996, **164**, 44–53.